View metadata, citation and similar papers at core.ac.uk

brought to you by CORE

provided by OpenSIUC

Southern Illinois University Carbondale
OpenSIUC

Articles

Department of Electrical and Computer Engineering

Spring 1-10-2010

Effect of lithotripter focal width on stone comminution in shock wave lithotripsy

Jun Qin
Southern Illinois University Carbondale, jqin@siu.edu

W. Neal Simmons
Duke University

Georgy Sankin
Duke University

Pei Zhong
Duke University

Follow this and additional works at: http://opensiuc.lib.siu.edu/ece_articles
Copyright 2010 Acoustical Society of America. This article may be downloaded for personal use only. Any other use requires prior permission of the author and the Acoustical Society of America.

Recommended Citation
Qin, Jun, Simmons, W. N., Sankin, Georgy and Zhong, Pei. "Effect of lithotripter focal width on stone comminution in shock wave lithotripsy." *Journal of Acoustical Society of America* 127, No. 4 (Spring 2010): 2635-2645. doi:10.1121/1.3308409.

This Article is brought to you for free and open access by the Department of Electrical and Computer Engineering at OpenSIUC. It has been accepted for inclusion in Articles by an authorized administrator of OpenSIUC. For more information, please contact opensiuc@lib.siu.edu.

Effect of lithotripter focal width on stone comminution in shock wave lithotripsy

Jun Qin,[a] W. Neal Simmons, Georgy Sankin, and Pei Zhong[b]
Department of Mechanical Engineering and Materials Science, Duke University, Durham, North Carolina 27708

(Received 30 July 2009; revised 8 January 2010; accepted 8 January 2010)

Using a reflector insert, the original HM-3 lithotripter field at 20 kV was altered significantly with the peak positive pressure (p_+) in the focal plane increased from 49 to 87 MPa while the −6 dB focal width decreased concomitantly from 11 to 4 mm. Using the original reflector, p_+ of 33 MPa with a −6 dB focal width of 18 mm were measured in a pre-focal plane 15-mm proximal to the lithotripter focus. However, the acoustic pulse energy delivered to a 28-mm diameter area around the lithotripter axis was comparable (~120 mJ). For all three exposure conditions, similar stone comminution (~70%) was produced in a mesh holder of 15 mm after 250 shocks. In contrast, stone comminution produced by the modified reflector either in a 15-mm finger cot (45%) or in a 30-mm membrane holder (14%) was significantly reduced from the corresponding values (56% and 26%) produced by the original reflector (no statistically significant differences were observed between the focal and pre-focal planes). These observations suggest that a low-pressure/broad focal width lithotripter field will produce better stone comminution than its counterpart with high-pressure/narrow focal width under clinically relevant *in vitro* comminution conditions.
© *2010 Acoustical Society of America.* [DOI: 10.1121/1.3308409]

PACS number(s): 43.80.Gx [CCC] Pages: 2635–2645

I. INTRODUCTION

The design of shock wave lithotripters has evolved significantly since the introduction of the original Dornier HM-3 in the early 1980s, which instantaneously revolutionized the surgical management for kidney and upper urinary stone diseases (Chaussy and Fuchs, 1989; Rassweiler *et al.*, 2005). The original HM-3 (first-generation lithotripter) was designed based on electrohydraulic principle using an underwater spark discharge for shock wave generation and a truncated ellipsoidal reflector for wave focusing. Patients were immersed in a large water tub filled with degassed/deionized water (37 °C) for acoustic coupling. Stone location was realized with bi-planar fluoroscopy. The initial success of the HM-3 prompted several manufacturers to introduce a number of second-generation lithotripters in the late 1980s, using different techniques for shock wave generation, wave focusing, and patient coupling (Rassweiler *et al.*, 1992; Lingeman, 1997). Representative second-generation lithotripters include the Siemens Lithostar, which uses an electromagnetic generator with an acoustic lens, both enclosed in a water cushion (i.e., "dry" lithotripter); and the Richard Wolf Piezolith-2300 that utilizes a self-focusing piezoelectric generator placed at the bottom of a small water basin. The primary changes in the design of the second-generation lithotripters are the increased aperture angle of the shock wave source and reduced acoustic output energy (Coleman and Saunders, 1989), enabling shock wave lithotripsy (SWL) to be performed under intravenous sedation rather than regional or general anesthesia as used for the HM-3 (Lingeman *et al.*, 2003). Continued evolution in lithotripter design in the 1990s led to the introduction of the third-generation lithotripters, which are characterized by high peak pressure with small focal width (or beam size; these two terms are used interchangeably hereinafter), increased energy output, as well as multifunctional use of the lithotripter system for SWL, ureteroscopic, and percutanous procedures (Lingeman, 1997; Rassweiler *et al.*, 2005). However, it should be noted that the technical improvements in the second- and third-generation lithotripters were largely made based on empirical experience, practical concerns for user convenience, and the desire for multifunctionality of the system rather than a rigorous understanding of the working mechanisms of SWL (Lingeman *et al.*, 2003; Zhou *et al.*, 2004; Zhong, 2007).

Previous studies have suggested that the progressive disintegration of kidney stones in SWL is produced by dynamic fatigue (Lokhandwalla and Sturtevant, 2000) under the influence of lithotripter shock wave (LSW) induced stress waves (e.g., by squeezing) inside the stone (Eisenmenger, 2001; Cleveland and Sapozhnikov, 2005) and cavitation bubbles in the surrounding fluid (Coleman *et al.*, 1987; Crum, 1988; Sass *et al.*, 1991; Zhong and Chuong, 1993; Zhong *et al.*, 1993; Pishchalnikov *et al.*, 2003). When stone phantoms of spherical geometry are used, the initial fracture of a stone may be enhanced by spallation at the posterior surface of the stone due to acoustic impedance mismatch and geometric focusing (Gracewski *et al.*, 1993; Xi and Zhong, 2001) and/or shear stresses produced by quasi-static or dynamic squeezing (Xi and Zhong, 2001; Cleveland and Sapozhnikov, 2005; Sapozhnikov *et al.*, 2007). It has been shown that stress wave-induced fracture is important for the initial dis-

[a]Present address: College of Engineering, Southern Illinois University Carbondale, Carbondale, IL 62901.
[b]Author to whom correspondence should be addressed. Electronic mail: pzhong@duke.edu

Author's complimentary copy

integration of kidney stones while cavitation is necessary to produce small and dischargeable fragments that are critical for the clinical success of SWL (Zhu *et al.*, 2002). Stress waves and cavitation interact synergistically to produce effective stone fragmentation during SWL (Zhu *et al.*, 2002; Sapozhnikov *et al.*, 2007; Zhong, 2007).

A growing number of clinical studies have demonstrated that compared to the original HM-3 lithotripter, the second- and third-generation lithotripters are often less effective in stone comminution yet have a higher propensity for tissue injury and stone recurrence (Graber *et al.*, 2003; Lingeman *et al.*, 2003; Gerber *et al.*, 2005). Among multiple potential contributory factors, a distinct change in the lithotripter design that has often been speculated to link with the reduced effectiveness of the third-generation lithotripters is the significantly increased peak pressure with concomitantly decreased beam size (Lingeman *et al.*, 2003).

In the past few years, there is a renewed interest in lithotripters with broad beam size, which is motivated primarily by the clinical success of Eisenmenger *et al.*'s (2002) "wide-focus and low-pressure" electromagnetic shock wave lithotripter that produces a peak positive pressure of 25 MPa and a −6 dB beam size of 18 mm. It should be noted that a low pulse repetition frequency (PRF) of 0.3 Hz was used in this initial series of clinical studies, which might contribute to the effective comminution outcome (Sapozhnikov *et al.*, 2002; Pishchalnikov *et al.*, 2006). Moreover, based on numerical model calculations, Cleveland and Sapozhnikov (2005) demonstrated that the peak principal stresses inside a stone increase significantly with the −6 dB focal width of the lithotripter. However, investigation of the effect of beam size on stone comminution using different lithotripters is problematic because of the inherent differences in the acoustic field, coupling method, stone localization technique, and output setting used by different lithotripters (Cleveland and McAteer, 2007). Much more work is still needed to better understand the effect of beam size on stone comminution and to define the optimal beam size for producing effective stone comminution with less tissue injury in SWL.

In this study, we have developed a method to modify the reflector geometry of the original HM-3 to produce a lithotripter field with high peak pressure and narrow beam size. Using this design, the effect of beam size on stone comminution can be compared in the same lithotripter using identical energy source, focusing technique, and coupling and stone localization methods, thus eliminating the inherent variations when such a comparison is performed using different lithotripters. Moreover, we have designed a new stone holder that allows us to mimic more closely the characteristics of stone fragmentation *in vivo*. Our results suggest that under the same effective acoustic pulse energy, a lithotripter field with low peak pressure and broad beam size produces significantly better stone comminution than its counterpart of high peak pressure and narrow beam size when stone fragments are allowed to disperse laterally as typically occurred *in vivo* during clinical SWL.

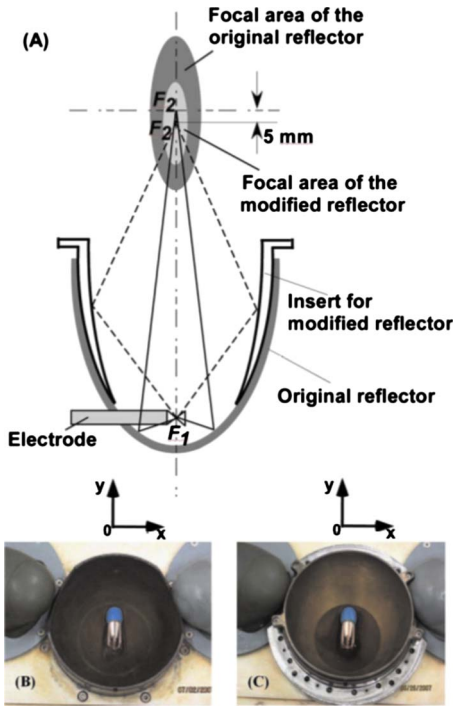

FIG. 1. (Color online) A schematic illustrating the original and modified reflector configurations in an HM-3 lithotripter (A), and photos of the original (B) and modified (C) reflectors.

II. MATERIALS AND METHODS

A. Lithotripter

The experiments were carried out in an original HM-3 lithotripter with an 80-nF capacitor and a truncated ellipsoidal brass reflector with a semi-major axis $a=138$ mm, a semi-minor axis $b=77.5$ mm, and a half-focal length $c=114$ mm. The HM-3 was operated at a representative clinical output setting of 20 kV with 1 Hz PRF.

To produce an acoustic field with high peak pressure and narrow beam size, a thin shell ellipsoidal brass reflector insert ($a'=134.4$ mm, $b'=75$ mm, and $c'=111.5$ mm) was fabricated and fitted snugly into the original HM-3 reflector (Fig. 1). The reflector insert shares the same first focus (F_1) with the original HM-3 reflector, yet its second focus (F_2') is located 5 mm pre-focally from the focus (F_2) of the original HM-3 reflector (Zhong and Zhou, 2001). The interpulse delay time Δt between the leading shock wave produced by the reflector insert and the second shock wave produced by the uncovered bottom surface of the original reflector can be determined by

$$\Delta t = \frac{2[(a-a')-(c-c')]}{c_0}, \tag{1}$$

where c_0 is the sound speed in water. Using the geometry of this new reflector insert [which is different than the one reported previously (Zhong and Zhou, 2001)], Δt is estimated to be about 1.5 μs. Because of nonlinear wave propagation, the leading shock wave and the second shock wave merge as they propagate toward the lithotripter focus, leading to the formation of an acoustic field with high peak pressure and narrow beam size (Zhou and Zhong, 2006).

Author's complimentary copy

B. Pressure measurements, energy density, and acoustic pulse energy calculations

The acoustic field and pressure distribution produced by the HM-3 using the original reflector in the focal plane ($z=0$ mm) and a pre-focal plane ($z=-15$ mm), as well as using the modified reflector in the focal plane, were determined by using a light spot hydrophone (LSHD-2, University of Erlangen-Nuremberg, Erlangen, Germany), which has a bandwidth of 40 MHz, a sensitivity of 10 mV/MPa, and spatial resolution of 100 μm, based on manufacturer's specification. The optical head of the LSHD (a $90\times60\times30$ mm^3 in $L\times W\times H$ glass block) was attached to a three-dimensional (3D) translation stage (Velmex, Bloomfield, NY) with the front surface of the glass block aligned perpendicular to the lithotripter axis. Alignment of the LSHD with F_2 was aided by a mechanical pointer. Using a LABVIEW program, the LSHD was scanned orthogonally from -14 to $+14$ mm in the measurement plane along the x- and y-axis, respectively (Fig. 1). The x-axis is defined by the left to right direction, and the y-axis is defined by the head to foot direction of the patient placed in the HM-3 tub. A step size of 1 mm was used between -6 and 6 mm, and a step size of 2 mm was used otherwise. At least six pressure waveforms at each selected position were recorded by using a digital oscilloscope (LeCroy 9314M, Chestnut Ridge, NY) operated at a sampling rate of 100 MHz. The oscilloscope was triggered by the spark discharge at the tip of the HM-3 electrode. To avoid cavitation interference, a long interpulse delay of 120 s was used for pressure measurement. Based on the measured pressure waveforms, several characteristic parameters of the lithotripter fields were calculated following the IEC 61846 Standard (IEC-Standard, 1998), unless otherwise specified. The -6 dB beam size in each measurement plane was determined by the focal width at half maximum of the peak positive acoustic pressure (p_+).

The energy density (ED) (or the derived pulse-intensity integral) of the lithotripter field at each measurement point is calculated by

$$\mathrm{ED}=\frac{1}{Z}\int_T p^2dt, \tag{2}$$

where $Z(=\rho c_0)$ is the acoustic impedance of the medium and ρ is the density of water, T is the total temporal integration limits ranging from the start to the end of the pressure waveform of the LSW, and p is the acoustic pressure that varies with time (t).

The derived acoustic pulse energy (E_R) of the LSW can be calculated by

$$E_R=\frac{1}{Z}\int_S\int_T p^2dtds=\int_S EDds, \tag{3}$$

where S is the measurement area. To determine E_R in different focal areas in each measurement plane, the integration was carried out over circular areas of 6-, 12-, and 28-mm diameters, respectively.

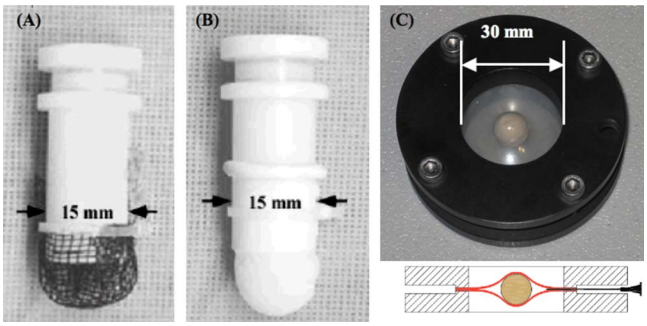

FIG. 2. (Color online) Pictures illustrating three different types of stone holders: (A) a mesh holder, (B) a finger cot holder, and (C) a membrane holder together with a schematic of its cross-sectional view. A 22 G needle (Becton Dickinson, Franklin Lakes, NJ) was sandwiched between the two silicone sheets in the membrane holder to equalize the pressure inside the exposure chamber with the fluid in the test tank.

C. Cavitation assessment

Cavitation activity produced in the lithotripter field was characterized using several established methods, including measurements by a 2.25-MHz focused hydrophone aligned confocally with F_2, by a pressure transducer (119B, PCB Piezotronics Inc., Depew, NY) placed in the measurement plane along the lithotripter axis, and by high-speed imaging using a phantom camera (Phantom v. 7.3, Vision Research, Wayne, NJ) at a framing rate up to 20 000 frames/s and an exposure time of 6 μs. The detailed description of these measurements can be found in our previous studies (Zhong *et al.*, 1997, 2001; Sankin *et al.*, 2005). In addition, cavitation potential in a lithotripter field (Iloreta *et al.*, 2007) was calculated using the Gilmore model assuming spherical symmetry in bubble geometry

$$R\left(1-\frac{U}{C}\right)\frac{dU}{dt}+\frac{3}{2}\left(1-\frac{U}{3C}\right)U^2=\left(1+\frac{U}{C}\right)H+\frac{1}{C}\left(1-\frac{U}{C}\right)R\frac{dH}{dt}, \tag{4}$$

where R and U are radius and velocity of the bubble wall, and C and H are the speed of sound in the liquid at the bubble wall and the enthalpy difference between the liquid at pressure on bubble wall and pressure at infinity. The numerical calculation was described previously (Zhu and Zhong, 1999).

D. Stone fragmentation tests

1. Stone holders

As shown in Fig. 2, three different types of stone holders were used in this study: (1) a 15-mm mesh holder, (2) a 15-mm finger cot holder, and (3) a 30-mm membrane holder. The mesh holder [Fig. 2(A)] is made of a plastic-mesh with 2-mm grids, which is fastened on a 15-mm plastic tube. During SWL, small fragments can fall through the 2-mm grids, while large residual fragments are kept within a relatively small area near the bottom of the mesh. The finger cot holder consists of a finger cot made of disposable rubber (QRP, Tucson, AZ), which is attached to the 15-mm tube [Fig. 2(B)]. Using the finger cot holder, stone fragments during

Author's complimentary copy

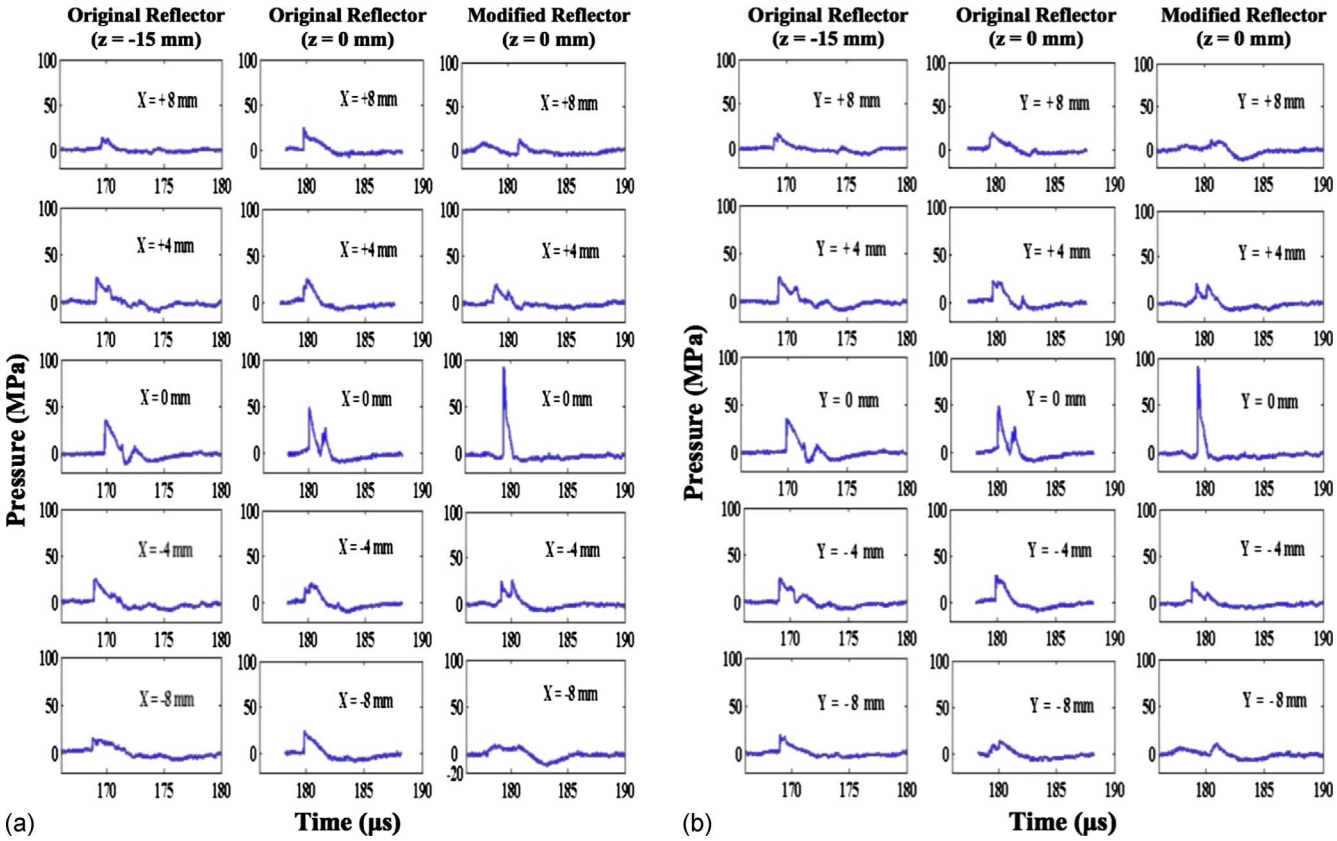

FIG. 3. (Color online) Representative pressure waveforms measured along the x-axis (A) and y-axis (B) in the focal (z=0 mm) and pre-focal (z=−15 mm) planes of the HM-3 lithotripter at 20 kV using either the original or modified reflector.

SWL will be retained and accumulated in a relatively small volume around the lithotripter focus. Overall, the mesh holder and finger cot represent idealized targeting of the stone during SWL.

The membrane holder consists of two Noryl polyphenylene oxide (PPO) plastic rings with an inner diameter of 30 mm, which compress two 0.5-mm thick transparent silicone rubber membranes (Product No.: 86915 K12, McMaster-Carr, Santa Fe Springs, CA) to sandwich a stone at the center of the holder [Fig. 2(C)]. The membrane holder allows stone fragments to disperse laterally, and thus mimicking more closely the lithotripsy procedures *in vivo*. An added benefit of the membrane holder is that the dynamic process of stone fragmentation during SWL can be recorded for further analysis.

2. Comminution tests

Spherical stone phantoms (D=10 mm) made of Begostone with a powder to water mixing ratio of 5:1 by weight (Liu and Zhong, 2002) were used. For comminution tests, a sample size of n=6 was used in each group. Before shock wave treatment, each stone phantom was weighed in dry state, and then immersed in degassed water for at least 4 h. Next, the stone phantom was placed into the selected holder filled with degassed water (O_2 concentration <3 mg/l), and aligned to F_2 under the guidance of bi-planar fluoroscopy. For treatment in the pre-focal plane, the stone phantom was first aligned to F_2, and then translated by 15 mm toward the shock wave source along the lithotripter axis using a 3D stage. After the shock wave treatment, all residual fragments were carefully collected, and then let dry in air for 24 h. Finally, the dry fragments were sieved sequentially through a series of grids of 2, 2.8, and 4 mm, respectively, and weighed thereafter. The efficiency of stone comminution was determined by the percent of fragments less than 2 mm.

III. RESULTS

A. Lithotripter fields

1. Pressure waveforms

Representative pressure waveforms measured on the beam axis and at ±4 and ±8 mm along the x- and y-axis in the three selected measurement planes are shown in Fig. 3. For the original reflector, the LSW arrives at the pre-focal location (z=−15 mm) on the beam axis in about 170 μs and at F_2 (z=0 mm) in about 180 μs after the spark discharge. A dual-peak structure in the leading compressive wave is observed at both locations, which is presumably caused by the truncation in the lateral sides of the ellipsoidal reflector to facilitate the bi-planar fluoroscopic imaging for stone localization (Zhou and Zhong, 2003). In comparison, the LSW produced by the modified reflector arrives at F_2 in about 179 μs after the spark discharge and its pressure waveform has a single peak with high pressure in the leading compressive wave. Away from F_2, two positive peaks can be observed in the LSW profile, and the peak pressure drops quickly along both the x- and y-axis. Specifically, p_+ produced by the modified reflector at F_2 nearly doubles the

Author's complimentary copy

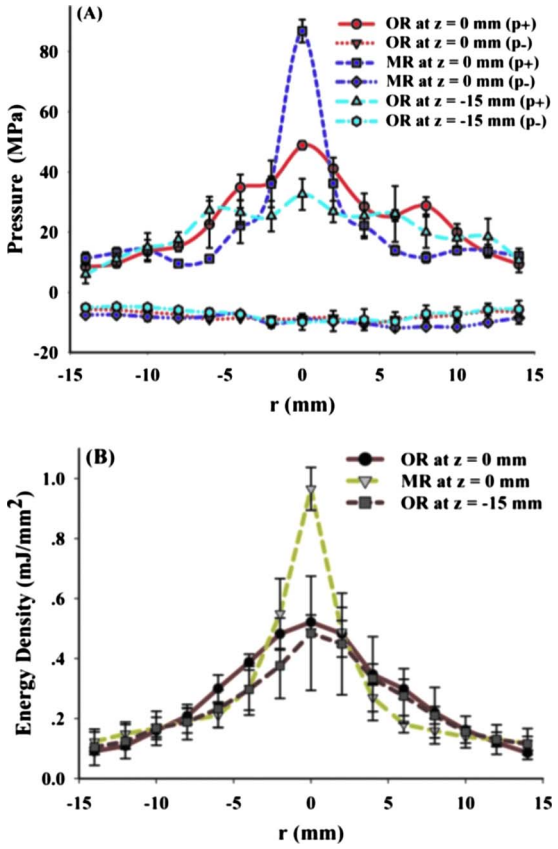

FIG. 4. (Color online) Peak pressure (A) and energy density (B) distribution of the shock waves produced by the HM-3 lithotripter at 20 kV using the OR in both the focal (z=0 mm) and pre-focal (z=−15 mm) planes, and the MR in the focal plane (z=0 mm).

value produced by the original reflector. However, at 4-mm lateral distance from F_2, the modified reflector produces a lower peak positive pressure than the original one [p =0.002 based on data shown in Fig. 4(A)].

Figure 4(A) shows the lateral distribution of p_+ and peak negative pressure (p_-) produced by the original reflector (OR) in the focal plane (z=0 mm) and in the pre-focal plane (z=−15 mm), as well as by the modified reflector (MR) in the focal plane of the HM-3 at 20 kV. The peak pressure at each radial distance was determined by the arithmetic mean of the corresponding values measured on the x- and y-axis at the same radial distance. In the focal plane and at a small radial distance from F_2 (i.e., −2 to 2 mm), the modified reflector produces much higher p_+ than the corresponding value of the original reflector, both of which are higher than the p_+ produced by the original reflector in the pre-focal plane (z=−15 mm). However, moving further away from F_2, p_+ of the modified reflector was found to be significantly lower than the corresponding values produced by the original reflector in both the z=0 mm and z=−15 mm planes. Specifically, the mean value of p_+ produced by the modified reflector at F_2 was measured to be 86.9 MPa, which is significantly higher than the corresponding value of 48.9 MPa produced by the original reflector ($p<0.001$). In the pre-focal plane, p_+ produced by the original reflector is further reduced to 32.6 MPa. In contrast to the significant change in p_+, the values of p_- were found to be similar, which are −10.6 MPa for the modified reflector in the focal plane, and −10.7 MPa in the focal plane and −9.8 MPa in the pre-focal plane for the original reflector. More importantly, the modified reflector produces the narrowest −6 dB beam size of 3.6 mm, while the original reflector produces a broad beam size of 10.9 mm in the focal plane, and the broadest beam size of 17.8 mm in the pre-focal plane.

2. Energy density and acoustic pulse energy

The distribution of energy density produced by the original and modified reflectors in the three aforementioned measurement planes is shown in Fig. 4(B). In general, the profiles of energy density variation produced by the two reflectors are similar to those in the peak positive pressure distribution [Fig. 4(A)]. One feature worth noting is that with the significant change in p_+ at F_2, the maximum energy density is increased from 0.52 $\mathrm{mJ/mm^2}$ produced by the original reflector to 0.97 $\mathrm{mJ/mm^2}$ produced by the modified reflector.

The acoustic pulse energy (E_R) is an important parameter of the lithotripter field that correlates closely with stone comminution in SWL (Granz and Kohler, 1992; Delius *et al.*, 1994). Based on pressure measurement data, E_R was calculated in three different cross-sectional areas of 6, 12, and 28 mm in diameter, respectively. It was found that E_R delivered to the three aforementioned measurement planes (i.e., 121.7, 115.9, and 116.1 mJ) is approximately the same in the area with 28-mm diameter, which covers essentially the area of the membrane holder. For the acoustic pulse energy that covers the 10-mm spherical stone (i.e., E_R in the 12-mm diameter area), the value produced by the original reflector in the focal plane (42.9 mJ) is slightly higher than the value (36.4 mJ) in the pre-focal plane, and that produced by the modified reflector in the focal plane (37.4 mJ). In comparison, near the beam axis (i.e., E_R in the 6-mm diameter area), the modified reflector produces the highest acoustic pulse energy (15.5 mJ), followed by the original reflector in the focal plane (13.0 mJ) and the pre-focal plane (11.2 mJ), respectively. Altogether, these results indicate that while the total acoustic pulse energy delivered to the membrane holder (i.e., E_R in the 28-mm diameter area) is essentially the same, the energy density and energy distribution can change significantly depending on the reflector configuration and the measurement plane. Overall, the modified reflector produces a narrow beam size and concentrates more acoustic energy around the beam axis, while the original reflector has a broad beam size with a comparably more uniform energy density distribution. The characteristic parameters of the acoustic fields produced by the original and modified reflectors in the three aforementioned measurement planes are summarized in Table I.

B. Cavitation activities produced in different lithotripter fields

1. Collapse time of bubble cluster

Using the 2.25-MHz focused hydrophone or the PCB transducer, the collapse time (t_c) of bubble cluster induced around F_2 or near the beam axis in the pre-focal plane was determined by the time delay between the arrival of the LSW

Author's complimentary copy

TABLE I. Characteristic parameters of the acoustic fields produced by an HM-3 lithotripter with the original and modified reflectors (the geometry of the reflector is given in Sec. II).

	Original reflector at $z=-15$ mm	Original reflector at $z=0$ mm	Modified reflector at $z=0$ mm
Peak positive pressure (MPa)	32.6 ± 5.2	48.9 ± 1.3	86.9 ± 3.8
Peak negative pressure (MPa)	-9.8 ± 2.7	-10.7 ± 0.4	-10.6 ± 0.6
−6 dB focal width (mm)[a]	17.8	10.9	3.6
Acoustic pulse energy (mJ) (6-mm diameter)[a]	11.2	13.0	15.5
Acoustic pulse energy (mJ) (12-mm diameter)[a]	36.4	42.9	37.4
Acoustic pulse energy (mJ) (28-mm diameter)[a]	115.9	121.7	116.1

[a]Data were calculated based on the arithmetic mean of the value measured on the x- and y-axes.

and the peak pressure in acoustic emission signals produced by the violent collapse of cavitation bubbles (Coleman *et al.*, 1987; Zhong *et al.*, 1997). In free field, t_c for bubble clusters produced by the original reflector at F_2 is 324.9 ± 19.0 μs (mean $\pm$ standard derivation), which is comparable to that produced by the modified reflector at F_2 (318.0 ± 32.3 μs), while the corresponding value for the original reflector in the pre-focal plane is slightly higher (365.7 ± 42.6 μs). Near the boundary of the PCB transducer, the values for t_c of the bubble cluster produced by the original reflector are 659.0 ± 30.4 μs at F_2 and 698.1 ± 35.9 μs in the pre-focal plane. The corresponding value for the modified reflector at F_2 is 636.6 ± 12.1 μs. Overall, there is no statistical difference ($p > 0.10$) between the values of t_c for bubble clusters produced at the three aforementioned positions either in free field or near a solid boundary.

2. High-speed imaging of bubble dynamics

Representative high-speed imaging sequences of the bubble dynamics produced in degassed water (O_2 concentration about 2.4 mg/l) by a single shock using either the original or modified reflector are shown in Fig. 5. Following the passage of the LSW at F_2 (~180 μs), a cluster of bubbles was observed that expanded rapidly, and some individual bubbles near the lithotripter beam axis coalesced with each other during the maximum expansion of the bubbles between 385 and 495 μs. Subsequently, the bubbles collapsed violently to a minimal size, followed by a few rebounds. Based on images from 25 individual sequences, no statistically significant differences were observed in terms of the maximum bubble radius produced by the original and modified reflectors at the center of the three measurement planes (see inset in Fig. 6).

3. Gilmore model calculation of bubble dynamics

Based on the pressure waveforms measured at different radial distances from the beam axis, the Gilmore model was used to calculate the maximum bubble radius (R_{max}) at the corresponding positions. It was found that the values of R_{max} predicted by the Gilmore model in the three measurement planes are comparable on the beam axis (i.e., ~1.1 mm), which is confirmed by the experimental measurements based

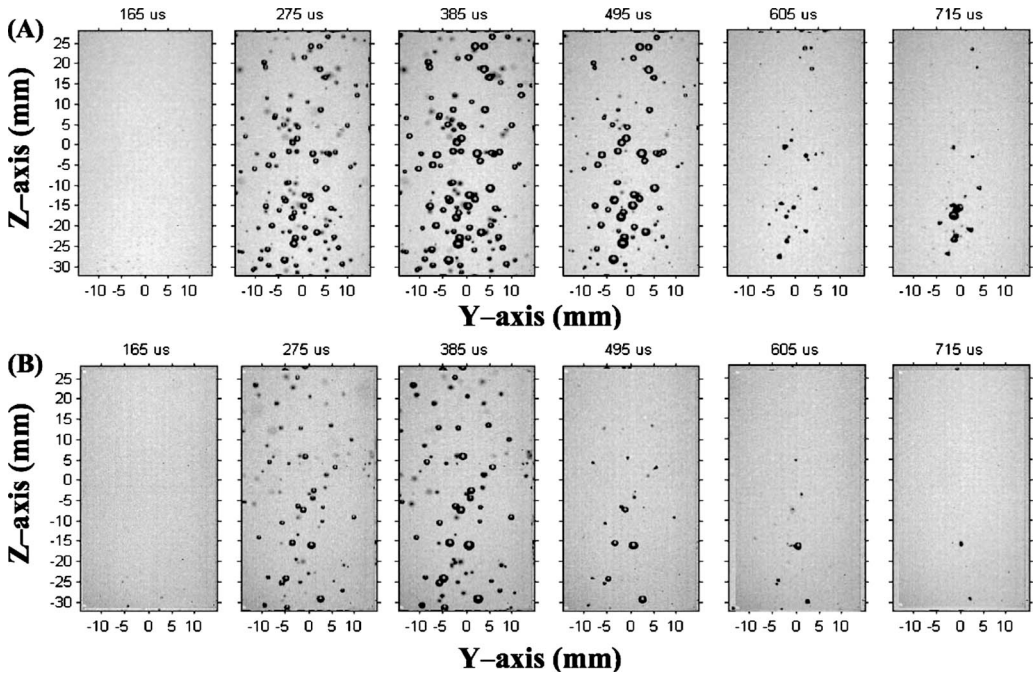

FIG. 5. Representative sequences of high-speed images of bubble dynamics in water produced by the HM-3 lithotripter at 20 kV using either the original (A) or the modified (B) reflector. The lithotripter focus is located at the origin of the coordinate system, frame size=60×30 mm^2 ($H \times W$), interframe time =110 μs, and O_2 concentration in water=2.4 mg/l. Time zero of the image sequence coincides with the spark discharge of the HM-3 electrode.

Author's complimentary copy

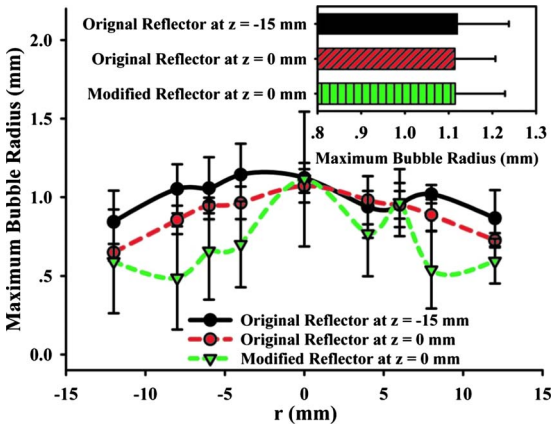

FIG. 6. (Color online) The maximum bubble radius predicted by the Gilmore model at different lateral distances from the central axis of the HM-3 lithotripter at 20 kV. The model calculation was carried out based on the pressure waveforms measured in the HM-3 lithotripter field using either the original or modified reflector. Inset shows the measured maximum bubble radius (mean ± standard derivation) from high-speed imaging sequences.

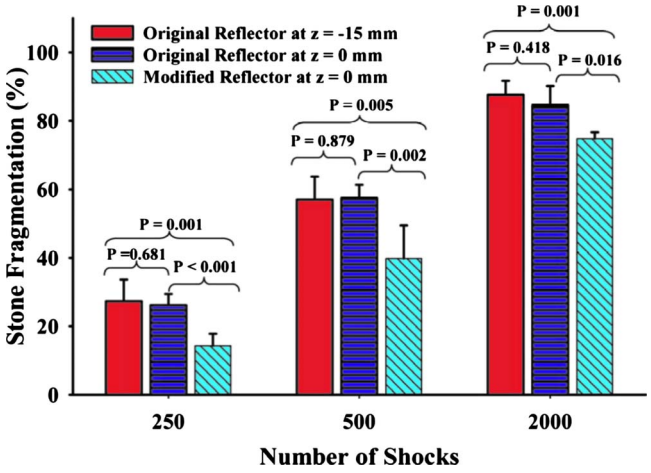

FIG. 8. (Color online) Dose-dependence of stone fragmentation in the membrane holder in the focal (z=0 mm) and pre-focal (z=−15 mm) planes produced by the HM-3 lithotripter at 20 kV using either the original or modified reflector.

on high-speed imaging (see inset in Fig. 6). Furthermore, for the original reflector, R_{max} was predicted to decrease slightly away from the beam axis both in the focal and pre-focal planes. In comparison, for the modified reflector, R_{max} was predicted to decrease significantly off the beam axis in the focal plane, although large standard deviations were observed.

C. Stone fragmentation

Stone comminution after 250 shocks produced by using either the original or modified reflector was evaluated in three different holders (Fig. 7). Overall, the efficiencies of stone fragmentation are the highest in the mesh holder, followed by in the finger cot, and the lowest values were obtained in the membrane holder. These differences can be attributed to the effects of LSW attenuation by the residual

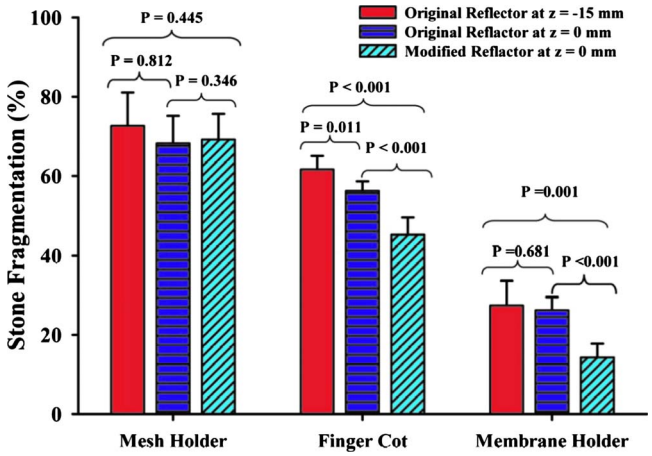

FIG. 7. (Color online) Stone fragmentation in the focal (z=0 mm) and pre-focal (z=−15 mm) planes after 250 shocks produced by the HM-3 lithotripter at 20 kV using either the original or modified reflector. The comminution tests were carried out in three different holders.

fragments in the finger cot (Zhu *et al.*, 2002) and the significant lateral spreading of stone fragments in the membrane holder (see Fig. 9).

In the mesh holder, no statistical differences in stone fragmentation were observed between the original reflector either in the focal or pre-focal plane and the modified reflector in the focal plane. In contrast, in the finger cot or in the membrane holder, the efficiencies of stone fragmentation produced by the modified reflector in the focal plane were found to be significantly lower (by more than 20%) than the corresponding values produced by the original reflector either in the focal or pre-focal plane. The differences are statistically significant ($p<0.001$). Altogether, these findings suggest that lithotripter beam size will not influence comminution outcome when small fragments (<2 mm) are filtered out and large fragments (>2 mm) are concentrated in a small volume around F_2 (as in the case of mesh holder). However, when residual fragments are accumulated inside the holder and/or spread to a large area (as in the case of finger cot and/or membrane holder), a lithotripter field with a broad beam size will produce better stone comminution than its counterpart with a narrow beam size under the same acoustic pulse energy.

Furthermore, the dose-dependency of stone comminution in the membrane holder was evaluated (Fig. 8). From 250 to 2000 shocks, the efficiencies of stone comminution produced by the original reflector both in the focal and pre-focal planes were found to be significantly higher than the corresponding values produced by the modified reflector in the focal plane ($p<0.02$). In comparison, there is no statistical difference ($p>0.4$) in stone fragmentation produced by the original reflector between the results obtained in the focal and pre-focal planes.

Figure 9(A) shows representative photographic sequences of stone comminution produced by the original reflector in the focal and pre-focal planes and by the modified reflector in the focal plane. These images were taken by a digital camera (Homeconnect 0770, 3Com, Marlborough, MA) mounted directly above the membrane holder, aiming at

Author's complimentary copy

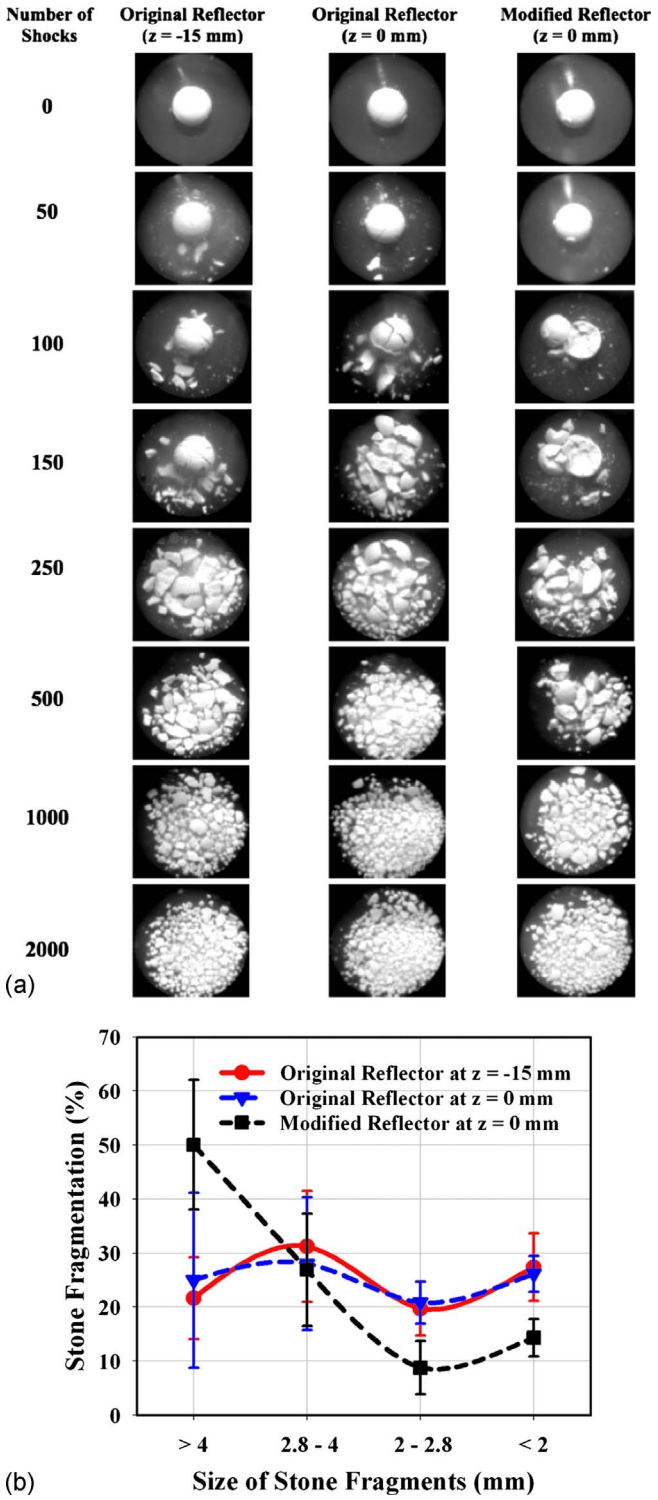

FIG. 9. (Color online) Representative images of the progressive stone comminution process from 0 to 2000 shocks (A) and fragment size distribution after 250 shocks (B) in the membrane holder in the focal (z=0 mm) and pre-focal (z=−15 mm) planes produced by the HM-3 lithotripter at 20 kV using either the original or modified reflector. Lithotripter shock waves were propagating in the direction out of the page.

the posterior surface of the stone. Several interesting features can be observed. First, using the original reflector, the initial fragmentation was observed to occur at the anterior side of the stone facing the incident LSW (see images after 50 shocks where multiple small pieces came off). With the membranes initially in contact with the spherical stone, cavitation damages such as the formation of deep craters centered around the lithotripter axis at the LSW entrance and exit sites, as often reported in free field (Pishchalnikov *et al.*, 2003), were not observed. Instead, the stone was crumbled from multiple sites into a cluster of fragments with relatively homogenous size distribution after 250 shocks [Fig. 9(B)]. In contrast, using the modified reflector, the initial fragmentation occurred primarily on the posterior side of the stone, with one or a few large pieces popping off from the backside of the stone within 100 shocks. In addition, the disintegration process was uneven and the resultant fragments have a relatively heterogeneous size distribution after 250 shocks, with a high percent of large fragment (>4 mm) with a concomitantly low percent of small fragment [<2.8 mm, see Fig. 9(B)]. This difference in the initial fragmentation of the stone produced by the original and modified reflectors may be related to the differences in pressure distribution and shock wave-bubble interaction produced by these two reflector configurations. Second, using the original reflector, the initial stone disintegration was observed to occur through multiple fracture planes (see images after 100 shocks in z=0 mm plane). In addition, because of the reduced peak positive pressure, the initiation of a significant disintegration of the stone in the pre-focal plane was slightly delayed compared to that in the focal plane. In comparison, using the modified reflector, the stone was fractured initially across a plane perpendicular to the beam axis into two large cap-like pieces, which were difficult to break in the subsequent 50 shocks (see images after 100 and 150 shocks in z=0 mm plane). Overall, the initial fragmentation process produced by the modified reflector in the focal plane is significantly slower than its counterparts produced by the original reflector both in the focal and pre-focal planes. Third, between 250 and 2000 shocks, large residual fragments were gradually broken up and spread over the entire area of the membrane holder in all three groups. Because of the higher pressure and stronger shock wave-bubble interaction, fragments located in the central area of the membrane holder were disintegrated much more easily than those located in the outer rim. Fourth, significant mixing of the fragments inside the membrane holder was observed during the treatment. Some fragments in the outer rim region were observed to migrate back to the central region and subsequently disintegrated, while other fragments were moved away from the central area and remained almost unchanged in the outer rim region. However, the mixing effect was not quantified. Overall, the characteristics of stone disintegration and fragment size distribution observed in these photographic sequences are consistent with the quantitative stone comminution results shown in Fig. 8.

IV. DISCUSSION

Since the introduction of the first-generation HM-3 lithotripter in the early 1980s, evolution in SWL technology has bought several significant changes in the design of modern lithotripsy systems (Lingeman, 1997; Rassweiler *et al.*, 2005). One of the most critical design changes in the second- and third-generation lithotripters is the increased aperture

Author's complimentary copy

and aperture angle of the shock wave source with concomitantly decreased beam size of the lithotripter field (Coleman and Saunders, 1989; Rassweiler *et al.*, 2005). Although it has been widely speculated that this dramatic reduction in beam size (by 50% or more) may significantly influence the effectiveness of stone comminution in SWL, an objective investigation of this topic using various lithotripsy devices is difficult. This is because of the inherent dissimilarities in the acoustic field, coupling method, stone localization technique, and output setting used by different lithotripters (Cleveland and McAteer, 2007). Ideally, such a study should be carried out in the same lithotripter to eliminate these inherent variations between different machines. Recently, the encouraging clinical results from Eisenmenger's "wide-focus and low-pressure" lithotripter (Eisenmenger, 2001; Eisenmenger *et al.*, 2002) and the introduction of "dual focus" design in clinical lithotripters (Leistner *et al.*, 2007) have further heightened the interest and urgency in addressing this critical issue.

To overcome the aforementioned limitation, we have developed a reflector insert for the HM-3 so that we can generate a significantly different lithotripter field with a high peak pressure (~87 MPa) and narrow beam size (~4 mm) compared to the original HM-3 lithotripter (49 MPa and 11 mm). These two distinctively different acoustic fields in the geometric focal plane ($z=0$ mm) of the HM-3 lithotripter are produced by using the same shock wave source and under the same output setting (i.e., 20 kV). Moreover, we have characterized the acoustic field produced by the original reflector in a pre-focal plane ($z=-15$ mm), which has an even lower peak pressure (~33 MPa) yet broader beam size (18 mm). Despite these differences, the effective acoustic pulse energies (i.e., E_R in the 12- and 28-mm diameter areas) produced by the original or modified reflector in the three aforementioned measurement planes are similar to each other within the uncertainty of the pressure measurements. Since acoustic pulse energy has been shown to correlate closely with stone comminution (Granz and Kohler, 1992; Delius *et al.*, 1994; Eisenmenger, 2001), our experimental system and study design provide a well-controlled test configuration to evaluate the effect of lithotripter beam size on stone comminution while avoiding potential confounding issues when such a comparison is made across different lithotripters.

Another critical limitation of previous *in vitro* studies is that stone is often placed either in a mesh holder or in a finger cot in which fragments smaller than certain size (e.g., 2 mm) are filtered out from the holder or confined within a small volume around the lithotripter focus. These phantom systems, while convenient and useful for quality control by the manufacturers to ensure adequate output of clinical lithotripters, do not capture some important characteristics of stone comminution *in vivo*, such as dispersion of fragments in the renal collecting system. To overcome this limitation, we have developed a membrane holder that allows stone fragments to be accumulated and also spread laterally within the holder ($D=30$ mm) during SWL. This membrane holder can also be used to record in real time the entire stone fragmentation process during SWL, providing valuable insights into the factors that may impact treatment outcome.

Using these phantom systems, we have observed that, using the same energy source and under comparable effective acoustic pulse energy, stone comminution produced in the mesh holder ($D=15$ mm) is similar and independent of the beam size. Because the stone was originally aligned with F_2 and, following each shock wave exposure, fragments less than 2 mm were filtered out from the mesh holder, the energy of ensuing LSWs could be delivered directly to residual fragments larger than 2 mm, leading to effective stone comminution (see Fig. 7). In contrast, when stone fragments were retained and confined within the finger cot ($D=15$ mm), the overall comminution efficiency was reduced substantially from the corresponding values in the mesh holder. Moreover, the largest reduction was observed with the modified reflector, which, because of its high $p+$, might experience the strongest attenuation of the LSW by residual small fragments accumulated at the bottom of the finger cot (Zhu *et al.*, 2002). It is also interesting to note that using the original reflector, stone comminution in the pre-focal position is slightly but significantly higher than that produced in the focal plane, which is interpreted as the result of stronger cavitation and more synergistic interaction between the stress waves and cavitation (Zhu *et al.*, 2002) produced in the finger cot at the pre-focal position than at the lithotripter focus. This finding is also consistent with the observation from a previous study (Sokolov *et al.*, 2002). Finally, stone comminution in the membrane holder was further reduced from the corresponding values in the mesh holder and in the finger cot. In comparison, the modified reflector produced significantly lower stone comminution than the original reflector, which, however, did not show a statistically significant difference between the results in the focal and pre-focal planes. These differences in stone comminution produced by the original and modified reflectors and the similarities between the focal and pre-focal planes in the original lithotripter field were further confirmed at various shock wave doses (see Fig. 8). Altogether, these findings suggest that when fragments are dispersed to a large area ($15\ \text{mm} < D < 30$ mm) during SWL, the original HM-3 with a broad beam size will produce better stone comminution than its counterpart of a narrow beam size produced by the modified reflector. However, further increase in the beam size (from 11 to 18 mm) with concomitantly reduced peak positive pressure (from 49 to 33 MPa) does not alter the resultant stone comminution in the membrane holder, indicating that an optimal beam size may exist that leads to effective stone comminution.

For the same effective acoustic pulse energy, why does a lithotripter field with a broad beam size (of ~11 mm) produce better stone comminution than its counterpart with a narrow beam size (of ~4 mm) under clinically relevant test conditions? Several interesting observations of the differences in stone fragmentation produced by the two contrasting lithotripter fields may be worth noting. First, a low-pressure/broad beam size lithotripter field breaks up stone initially on the anterior surface of the stone and the damage propagates through multiple fracture planes, resulting in fragments with a relatively homogeneous size distribution [see Fig. 9(B)]. This observation is consistent with other

Author's complimentary copy

studies using low-pressure and broad beam size lithotripters (Eisenmenger, 2001; Eisenmenger *et al.*, 2002). In contrast, a high-pressure/narrow beam size lithotripter field breaks up stone initially from the posterior side of the stone. This initial damage may be caused by the high pressure at the center and low pressure surrounding the periphery of the stone through a combination of spallation (Gracewski *et al.*, 1993; Xi and Zhong, 2001) and quasi-static or dynamic squeeze (Eisenmenger, 2001; Cleveland and Sapozhnikov, 2005; Sapozhnikov *et al.*, 2007) mechanism that causes an uneven fracture of the stone (see Fig. 9). Once the original spherical geometry of the stone is destroyed by the initial fracture, the residual large fragments with irregular geometry become much more resistant to subsequent shock waves, and the fragments produced by additional 150–200 shocks are heterogeneous in size distribution [see Fig. 9(B)]. Second, the radiation force exerted by the incident LSW may cause lateral displacement of stone fragments. This feature was observed but not quantified in this study. Especially, because of the high peak pressure and pressure gradient along the beam axis of the modified reflector, large residual fragments may be dispersed further away from the high-pressure and high ED region at the center of focal region. Significant lateral dispersion of the fragments may impact more negatively on stone comminution produced by the modified reflector because of its small effective fragmentation zone. However, significant mixing was observed in the membrane holder in the later stage of the stone comminution process, during which some fragments in the outer rim region could move back to the central area or vise versa. This mixing effect might affect stone fragmentation outcome in the membrane holder when a large number of shock waves were delivered. Nevertheless, the extent by which this mixing effect may occur *in vivo* is not known. Third, there are subtle differences in cavitation potential and bubble dynamics produced by the two lithotripter fields. Based on the results of high-speed imaging (Fig. 5) and model calculations (Fig. 6), the maximum bubble sizes produced by the two lithotripter fields are similar along the beam axis. However, at off-axis locations, the original reflector with a broad beam size may generate stronger cavitation than the modified reflector (see Fig. 6). Combined with the characteristics of pressure distribution [Fig. 4(A)], these observations suggest that a high-pressure/narrow beam size lithotripter field will be effective in comminuting stones that are accurately aligned to the lithotripter focus, and when the residual fragments are also confined in a small volume around the beam focus under the influence of minimal respiratory motion. In comparison, a low-pressure/broad beam size lithotripter field will be more effective when stones are less accurately aligned with the beam focus, and when residual fragments are dispersed or moved away from the lithotripter axis due to significant respiratory motion.

It has been argued that with high-pressure and high-energy output, a small beam size lithotripter may produce the same effective fragmentation zone based on an absolute pressure threshold (e.g., $p_+ = 10$ MPa) for stone comminution, compared to a low-pressure and broad beam size lithotripter such as the HM-3 (Wess, 2005). This argument, however, is primarily based on stone fragmentation data obtained under idealized test conditions such as in a mesh holder or finger cot placed at the lithotripter focus (Teichman *et al.*, 2000). In addition, the output settings used by different lithotripters in those previous studies are not the same, with significantly higher acoustic pulse energy delivered by the high-pressure and narrow beam size third-generation lithotripters, leading to better treatment output under idealized test conditions (Teichman *et al.*, 2000). In contrast, under clinically relevant *in vitro* test conditions such as stone fragmentation in the membrane holder as described in this study, which accounts for dispersion of stone fragments, or in a setup that mimics the respiratory motion of the stone (Cleveland *et al.*, 2004), the comminution efficiency produced by a lithotripter field with high peak pressure and narrow beam size has been found to be greatly reduced. These factors (i.e., dispersion of stone fragments and respiratory motion of the stone) may also contribute to the reduced comminution efficiency with concomitantly increased stone recurrence rate observed clinically in the third-generation lithotripters with high pressure and narrow beam size (Lingeman *et al.*, 2003; Gerber *et al.*, 2005). Furthermore, comparison of stone comminution based on absolute pressure threshold (instead of effective acoustic pulse energy delivered to the patient) without considering the adverse effects of high-energy shock waves on renal tissues should not be recommended for guiding the clinical practice of SWL. Similar to stone comminution, it is well known that tissue injury in SWL increases with the output energy of the lithotripter (Evan *et al.*, 1998).

In summary, we have developed a method to modify the reflector geometry of the original HM-3 lithotripter so that a distinctively different acoustic field with high pressure and narrow beam size can be produced using the same energy source and output setting. For the same effective acoustic pulse energy, a lithotripter field with low peak pressure and broad beam size produces significantly better stone comminution than its counterpart of high peak pressure and narrow beam size when stone fragments are dispersed laterally as frequently occurs *in vivo* during clinical SWL. A high-pressure and narrow beam size lithotripter field produces efficient comminution when stone and residual fragments are well constrained near the lithotripter focus. On the other hand, their fragmentation power decreases rapidly at off-axis positions. In contrast, a low pressure and broad beam size, lithotripter field produces effective stone comminution over a large area and the resultant fragments are relatively homogeneous and small in size.

ACKNOWLEDGMENTS

This work was supported in part by NIH through Grant Nos. R01-DK052985 and S10-RR16802. The authors are also grateful to W. Eisenmenger, M. Delius, and R. Nanke for their critical reading of the manuscript and helpful discussions.

Chaussy, C. G., and Fuchs, G. J. (**1989**). "Current state and future-developments of noninvasive treatment of human urinary stones with extracorporeal shock-wave lithotripsy," J. Urol. (Baltimore) **141**, 782–789.
Cleveland, R. O., Anglade, R., and Babayan, R. K. (**2004**). "Effect of stone motion on in vitro comminution efficiency of Storz Modulith SLX," J. Endourol **18**, 629–633.

Author's complimentary copy

Cleveland, R. O., and McAteer, J. A. (**2007**). "The physics of shock wave lithotripsy," in *Smith's Textbook of Endourology*, edited by A. D. Smith, G. H. Badlani, D. H. Bagley, H.Demetrius, R. V. Clayman, S. G. Docimo, and G. H. Jordan (BC Decker, Hamilton, ON, Canada), pp. 317–332.

Cleveland, R. O., and Sapozhnikov, O. A. (**2005**). "Modeling elastic wave propagation in kidney stones with application to shock wave lithotripsy," J. Acoust. Soc. Am. **118**, 2667–2676.

Coleman, A. J., and Saunders, J. E. (**1989**). "A survey of the acoustic output of commercial extracorporeal shock wave lithotripters," Ultrasound Med. Biol. **15**, 213–227.

Coleman, A. J., Saunders, J. E., Crum, L. A., and Dyson, M. (**1987**). "Acoustic cavitation generated by an extracorporeal shockwave lithotripter," Ultrasound Med. Biol. **13**, 69–76.

Crum, L. A. (**1988**). "Cavitation microjets as a contributory mechanism for renal calculi disintegration in ESWL," J. Urol. (Baltimore) **140**, 1587–1590.

Delius, M., Ueberle, F., and Gambihler, S. (**1994**). "Destruction of gallstones and model stones by extracorporeal shock-waves," Ultrasound Med. Biol. **20**, 251–258.

Eisenmenger, W. (**2001**). "The mechanisms of stone fragmentation in ESWL," Ultrasound Med. Biol. **27**, 683–693.

Eisenmenger, W., Du, X. X., Tang, C., Zhao, S., Wang, Y., Rong, F., Dai, D., Guan, M., and Qi, A. (**2002**). "The first clinical results of 'wide-focus and low-pressure' ESWL," Ultrasound Med. Biol. **28**, 769–774.

Evan, A. P., Willis, L. R., Lingeman, J. E., and McAteer, J. A. (**1998**). "Renal trauma and the risk of long-term complications in shock wave lithotripsy," Nephron **78**, 1–8.

Gerber, R., Studer, U. E., and Danuser, H. (**2005**). "Is newer always better? A comparative study of 3 lithotriptor generations," J. Urol. (Baltimore) **173**, 2013–2016.

Graber, S. F., Danuser, H., Hochreiter, W. W., and Studer, U. E. (**2003**). "A prospective randomized trial comparing 2 lithotriptors for stone disintegration and induced renal trauma," J. Urol. (Baltimore) **169**, 54–57.

Gracewski, S. M., Dahake, G., Ding, Z., Burns, S. J., and Everbach, E. C. (**1993**). "Internal stress wave measurements in solids subjected to lithotripter pulses," J. Acoust. Soc. Am. **94**, 652–661.

Granz, B., and Kohler, G. (**1992**). "What makes a shock wave efficient in lithotripsy?," J. Stone Dis. **4**, 123–128.

IEC-Standard (**1998**). "International Standard: Pressure pulse lithotripters—Characteristics of fields," IEC 61846.

Iloreta, J. I., Zhou, Y. F., Sankin, G. N., Zhong, P., and Szeri, A. J. (**2007**). "Assessment of shock wave lithotripters via cavitation potential," Phys. Fluids **19**, 086103.

Leistner, R., Wendt-Nordahl, G., Grobholz, R., Michel, M. S., Marlinghaus, E., Kohrmann, K. U., Alken, P., and Hacker, A. (**2007**). "A new electromagnetic shock-wave generator 'SLX-F2' with user-selectable dual focus size: Ex vivo evaluation of renal injury," Urol. Res. **35**, 165–171.

Lingeman, J. E. (**1997**). "Extracorporeal shock wave lithotripsy. Development, instrumentation, and current status," Urol. Clin. North Am. **24**, 185–211.

Lingeman, J. E., Kim, S. C., Kuo, R. L., McAteer, J. A., and Evan, A. P. (**2003**). "Shockwave lithotripsy: Anecdotes and insights," J. Endourol **17**, 687–693.

Liu, Y., and Zhong, P. (**2002**). "BegoStone—A new stone phantom for shock wave lithotripsy research," J. Acoust. Soc. Am. **112**, 1265–1268.

Lokhandwalla, M., and Sturtevant, B. (**2000**). "Fracture mechanics model of stone comminution in ESWL and implications for tissue damage," Phys. Med. Biol. **45**, 1923–1940.

Pishchalnikov, Y. A., McAteer, J. A., Williams, J. C., Pishchalnikova, I. V., and Vonderhaar, R. J. (**2006**). "Why stones break better at slow shockwave rates than at fast rates: In vitro study with a research electrohydraulic lithotripter," J. Endourol **20**, 537–541.

Pishchalnikov, Y. A., Sapozhnikov, O. A., Bailey, M. R., Williams, J. C., Jr., Cleveland, R. O., Colonius, T., Crum, L. A., Evan, A. P., and McAteer, J. A. (**2003**). "Cavitation bubble cluster activity in the breakage of kidney stones by lithotripter shockwaves," J. Endourol **17**, 435–446.

Rassweiler, J., Henkel, T. O., Kohrmann, K. U., Potempa, D., Junemann, K. P., and Alken, P. (**1992**). "Lithotripter technology—Present and future," J. Endourol **6**, 1–13.

Rassweiler, J. J., Tailly, G. G., and Chaussy, C. (**2005**). "Progress in lithotriptor technology," EAU Update Series **3**, 17–36.

Sankin, G. N., Simmons, W. N., Zhu, S. L., and Zhong, P. (**2005**). "Shock wave interaction with laser-generated single bubbles," Phys. Rev. Lett. **95**, 034501.

Sapozhnikov, O. A., Khokhlova, V. A., Bailey, M. R., Williams, J. C., McAteer, J. A., Cleveland, R. O., and Crum, C. A. (**2002**). "Effect of overpressure and pulse repetition frequency on cavitation in shock wave lithotripsy," J. Acoust. Soc. Am. **112**, 1183–1195.

Sapozhnikov, O. A., Maxwell, A. D., MacConaghy, B., and Bailey, M. R. (**2007**). "A mechanistic analysis of stone fracture in lithotripsy," J. Acoust. Soc. Am. **121**, 1190–1202.

Sass, W., Braunlich, M., Dreyer, H. P., Matura, E., Folberth, W., Preismeyer, H. G., and Seifert, J. (**1991**). "The mechanisms of stone disintegration by shock waves," Ultrasound Med. Biol. **17**, 239–243.

Sokolov, D. L., Bailey, M. R., Crum, L. A., Blomgren, P. M., Connors, B. A., and Evan, A. P. (**2002**). "Prefocal alignment improves stone comminution in shockwave lithotripsy," J. Endourol **16**, 709–715.

Teichman, J. M., Portis, A. J., Cecconi, P. P., Bub, W. L., Endicott, R. C., Denes, B., Pearle, M. S., and Clayman, R. V. (**2000**). "In vitro comparison of shock wave lithotripsy machines," J. Urol. (Baltimore) **164**, 1259–1264.

Wess, O. (**2005**). "Shock wave lithotripsy (SWL) and focal size," in *Therapeutic Energy Applications in Urology—Standards and Recent Developments*, edited by D. J. Ch. Chaussy, G. Haupt, K. U. Kohrmann, and D. Wilbert (Georg Thieme Verlag KG, Stuttgart, Germany), pp. 26–35.

Xi, X., and Zhong, P. (**2001**). "Dynamic photoelastic study of the transient stress field in solids during shock wave lithotripsy," J. Acoust. Soc. Am. **109**, 1226–1239.

Zhong, P. (**2007**). "Innovations in lithotripsy technology," in the 1st Annual International Urolithiasis Research Symposium, Indianapolis, IN, pp. 317–325.

Zhong, P., and Chuong, C. J. (**1993**). "Propagation of shock waves in elastic solids caused by cavitation microjet impact. I: Theoretical formulation," J. Acoust. Soc. Am. **94**, 19–28.

Zhong, P., Chuong, C. J., and Preminger, G. M. (**1993**). "Propagation of shock waves in elastic solids caused by cavitation microjet impact. II: Application in extracorporeal shock wave lithotripsy," J. Acoust. Soc. Am. **94**, 29–36.

Zhong, P., Cioanta, I., Cocks, F. H., and Preminger, G. M. (**1997**). "Inertial cavitation and associated acoustic emission produced during electrohydraulic shock wave lithotripsy," J. Acoust. Soc. Am. **101**, 2940–2950.

Zhong, P., and Zhou, Y. (**2001**). "Suppression of large intraluminal bubble expansion in shock wave lithotripsy without compromising stone comminution: Methodology and in vitro experiments," J. Acoust. Soc. Am. **110**, 3283–3291.

Zhong, P., Zhou, Y., and Zhu, S. (**2001**). "Dynamics of bubble oscillation in constrained media and mechanisms of vessel rupture in SWL," Ultrasound Med. Biol. **27**, 119–134.

Zhou, Y., Cocks, F. H., Preminger, G. M., and Zhong, P. (**2004**). "Innovations in shock wave lithotripsy technology: Updates in experimental studies," J. Urol. (Baltimore) **172**, 1892–1898.

Zhou, Y., and Zhong, P. (**2003**). "Suppression of large intraluminal bubble expansion in shock wave lithotripsy without compromising stone comminution: Refinement of reflector geometry," J. Acoust. Soc. Am. **113**, 586–597.

Zhou, Y., and Zhong, P. (**2006**). "The effect of reflector geometry on the acoustic field and bubble dynamics produced by an electrohydraulic shock wave lithotripter," J. Acoust. Soc. Am. **119**, 3625–3636.

Zhu, S., Cocks, F. H., Preminger, G. M., and Zhong, P. (**2002**). "The role of stress waves and cavitation in stone comminution in shock wave lithotripsy," Ultrasound Med. Biol. **28**, 661–671.

Zhu, S. L., and Zhong, P. (**1999**). "Shock wave-inertial microbubble interaction: A theoretical study based on the Gilmore formulation for bubble dynamics," J. Acoust. Soc. Am. **106**, 3024–3033.

Author's complimentary copy